Calculations of Nucleus-Nucleus Microscopic Optical Potentials and the Respective Elastic Differential and Total Reaction Cross Sections*

E. V. Zemlyanaya[1], K. V. Lukyanov[1], V. K. Lukyanov[1], I. N. Kukhtina[1], A. N. Antonov[2], K. M. Hanna[3], and B. Słowiński[4,5]

[1] Joint Institute for Nuclear Research, Dubna 141980, Russia
[2] Institute of Nuclear Research and Nuclear Energy, Bulgarian Academy of Sciences, Sofia 1784, Bulgaria
[3] Math. and Theor. Dept., NRC, Atomic Energy Authority, Cairo, Egypt
[4] Institute of Atomic Energy, Otwock-Swierk, Poland
[5] Faculty of Physics, Warsaw University of Technology, Poland

Abstract. The double-folding model and the high-energy approximation (HEA) of the microscopic theory of scattering are involved to construct the nucleus-nucleus optical potentials. In the framework of HEA, the role of the trajectory distortion and in medium effects on cross sections are estimated. Calculations of differential elastic and total reaction cross sections are presented and compared with experimental data. Data on reactions of exotic nuclei ^{6}He and ^{6,7}Li with ^{28}Si are analyzed. The co-called semimicroscopic potentials are introduced to get the best fit to experimental data. These potentials have two free parameters to adjust only strengths of the microscopically calculated real and imaginary parts of optical potentials.

1 Introduction

The heavy-ion microscopic optical potentials are requested, firstly, when developing technologies for processing radioactive wastes by means of irradiating them with heavy-ion beams. They needs in predictions of nucleus-nucleus total reaction cross sections, obtained in calculations by means of optical potentials.

Second, the nucleus-nucleus potentials are necessary to calculate distorted waves in the entrance and exit scattering channels for the following study of the peripheral inelastic scattering and direct nuclear reactions with transfers of nucleons.

Then, as compared to the phenomenological potentials that have an ambiguity in determining parameters, the microscopic potentials have no free parameters. These potentials can be used as templates for constructions of the so-called semimicroscopic optical potentials, depended on the energy and sort of colliding nuclei.

The other use of studying microscopic potentials is that in their construction one can get the information on dependence of nucleon-nucleon forces of the density of

* Partially support from the Russian Foundation for Basic Research (grant 03-01-00228) is gratefully acknowledged.

nuclear matter in overlapping region of colliding nuclei. These latter can help to explain saturation of nuclear matter and also to obtain the nuclear incompressibility value to be appropriate for the cold nuclear matter in neutron stars.

Below we show briefly the basic formulas for the double-folding potential which is used as a real part of an optical potential, and also for the complex potential (with the real and imaginary parts) obtained within the high-energy approximation (HEA). Then, they will be applied in calculations of differential elastic and total reaction cross sections made in the framework of the analytic HEA theory and [1,2], generalized for nucleus-nucleus scattering in [3, 4], and also by using the codes for numerical solving the Schrödinger equation DWUCK4 (for lower energies) [5] and ECIS (for higher energies) [6]. (Some details of such consideration of nucleus-nucleus scattering can be found in the review paper [7]).

2 Microscopic Nucleus-Nucleus Optical Potentials

In recent decade much efforts have gone into developing microscopic models for calculating nucleus-nucleus potentials themselves – first of all, the double-folding model (see, e.g., [8, 9]). The peculiar feature of the later is that it calculates only the real part of an optical potential while the imaginary part is usually presented phenomenologically with free parameters fitted to experimental data for each specific energy individually. On the contrary, the HEA microscopic eikonal phase of scattering and the corresponding amplitude and total reaction cross section can be calculated unambiguously using the following expressions[1]:

$$f(q) = ik \int_0^\infty J_0(qb) \left(1 - e^{i\Phi_N(b) + i\Phi_c(b)}\right) b\, db, \tag{1}$$

$$\sigma_r = 2\pi \int_0^\infty \left(1 - e^{-2Im\Phi_N(b)}\right) b\, db, \tag{2}$$

$$\Phi(b) = \bar{\sigma}_{NN}(i + \bar{\alpha}_{NN}) \frac{1}{4\pi} \int_0^\infty qdq\, J_0(qb)\, \tilde{\rho}_p(q)\, \tilde{\rho}_t(q)\, \tilde{f}_N(q)\, f_m. \tag{3}$$

Here $q = 2k\sin(\vartheta/2)$ is the momentum transfer, b is the impact parameter, and the eikonal phase is defined as an integral over the straight-line trajectory along the initial momentum $\mathbf{k}_i$. In (3), the real and imaginary parts depend on the collision energy through $\bar{\alpha}_{NN}$ and $\bar{\sigma}_{NN}$ - the isospin-averaged ratio of the real to imaginary parts of the NN-amplitude of scattering at forward angles and the NN total cross sections, respectively. They are known from experimental data on NN-scattering. Also, the known values are the form factors $\tilde{\rho}_{p(t)}(q)$ of the projectile and target nuclei, while $\tilde{f}_N(q)$ is the NN-scattering form factor, and f_m is the so-called in medium factor.

As was shown in [11], the HEA (3) corresponds unambiguously to the HEA optical potential

[1] The detailed consideration of HEA in terms of eikonal functions is presented, e.g., in [10]

$$U_{opt}^{H}(r) = V^{H}(r) + iW^{H}(r), \tag{4}$$

$$V^{H} = -\frac{2E}{k(2\pi)^2}\bar{\sigma}_{NN}\bar{\alpha}_{NN}\int_0^\infty dq\, q^2 j_0(qr)\tilde{\rho}_p(q)\tilde{\rho}_t(q)\tilde{f}_N(q), \tag{5}$$

$$W^{H} = -\frac{2E}{k(2\pi)^2}\bar{\sigma}_{NN}\int_0^\infty dq\, q^2 j_0(qr)\tilde{\rho}_p(q)\tilde{\rho}_t(q)\tilde{f}_N(q). \tag{6}$$

So, using the microscopic HEA potential $U_{opt}^{H} = V^{H} + iW^{H}$ one gets the same results of calculations as being obtained when applying the HEA amplitude (1) and reaction cross section (2) with the phase (3). This potential is characteristic for the nucleus-nucleus scattering at relatively high energies, in which case the structure of nuclei, including exchange effects, manifests itself predominantly in the peripheral region of interaction due to the strong absorption in the interior. Therefore the structure plays an important role in formation of the real part of optical potential in the region $r \geq R$. It is seen from (4)-(6) that the real and imaginary parts of the HEA potential have the same shape, the fact, which, in general, is not verified by the results of analysis of experimental data in the framework of the phenomenological many-parameter optical potentials.

Now we represent the real double-folding potential which includes dependence on energy and in medium effect (see, e.g., [8]):

$$V^{DF} = V^{D} + V^{EX} \tag{7}$$

$$V^{D}(r) = \int d^3r_p d^3r_t\, \rho_p(\mathbf{r}_p)\, \rho_t(\mathbf{r}_t)\, v_{NN}^{D}(s), \qquad \mathbf{s} = \mathbf{r} + \mathbf{r}_t - \mathbf{r}_p, \tag{8}$$

$$V^{EX}(r) = \int d^3r_p d^3r_t\, \rho_p(\mathbf{r}_p, \mathbf{r}_p + \mathbf{s})\, \rho_t(\mathbf{r}_t, \mathbf{r}_t - \mathbf{s}) \times v_{NN}^{EX}(s)\, \exp\left[\frac{i\mathbf{K}(r)\cdot s}{M}\right]. \tag{9}$$

Here $\rho_{p(t)}(\mathbf{r}_1, \mathbf{r}_2)$ are one-particle density matrices, while $\rho_{p(t)}(\mathbf{r})$ are their diagonal parts. The modern calculations of double-folding potentials apply the effective Paris nucleon-nucleon CDM3Y6 potential v_{NN} having the form

$$v_{NN}(E, \rho, s) = g(E)\, F(\rho)\, v(s), \quad v(s) = \sum_{i=1,2,3} N_i \frac{\exp(-\mu_i s)}{\mu_i s}, \tag{10}$$

where the energy and density dependences are given as

$$g(E) = 1 - 0.003E/A_p, \quad F(\rho) = C[1 + \alpha\exp(-\beta\rho) - \gamma\rho], \tag{11}$$

$$\rho = \rho_p + \rho_t, \quad C = 0.2658, \quad \alpha = 3.8033, \quad \gamma = 4.0,$$

and the parameters N_i and μ_i are given, e.g., in [8]. The energy dependence of V^{EX} arises primarily from the contribution of the exponent in the integrand, where

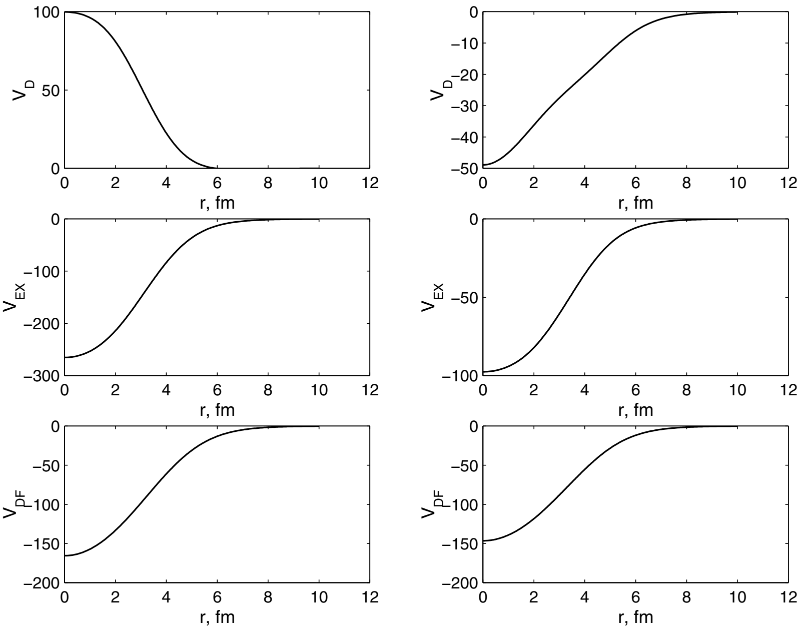

Figure **1.** Behavior of different terms and of the total nucleus-nucleus potentials calculated with the help of Paris (left side) and Reid (right side) effective NN-potentials.

$K(r) = \{2Mm/\hbar^2[E - V_N(r) - V_c(r)]\}^{1/2}$ is the local nucleus-nucleus momentum, $M = A_pA_t/(A_p + A_t)$; m is the nucleon mass, and therefore there occurs the typical non-linear problem.

Here we paid attention to the role of exchange effects in calculations of nucleus-nucleus real potentials. This is given in Figure 1 where the double-folding V^{DF}-potential for the ^{6}He+^{28}Si scattering at E=25 MeV/nucleon is calculated using two different kinds of effective v_{NN} potentials, the Paris CDM3Y6 and the Reid DDM3Y1 potentials. They have different sets of the parameters N_i, μ_i and C, α, β, γ (see [8]). It is seen, that their direct parts have different signs, and that the exchange part, in the case of CDM3Y6-forces, is negative and very strong. But in spite of different signs of separated terms V^D and V^{EX} of these two potentials, the sum of each pairs have the almost identical shape. So, for example, if one calculates only the direct part V^D by using the Paris M3Y NN-forces without accounting for the exchange part V^{EX}, then the nuclear potential occurs positive one. This demonstrates the very important role of exchange terms.

3 Total Reaction Cross Section and Attended Effects

In HEA, the total reaction cross section (2) depends on the imaginary part of the eikonal phase and can be directly calculated using eq.(3). Also, the same result is obtained if one uses the definition

$$\Phi(b) \;=\; -\frac{1}{\hbar v}\int_{-\infty}^{\infty} U(\sqrt{b^2+z^2})\,dz, \tag{12}$$

and utilizes the HEA optical potential (6). In both cases only the imaginary part of the potential is formally presented in calculations. Instead, if one uses the numerical codes of solving Schrödinger equation the real part of U_{opt} contributes, as well. In the HEA calculations, the effect of the real part can be accounted for by inclusion of the so-called trajectory distortion, when instead of integration in (1), (2) along the straight-line trajectory one uses the classical trajectory of motion calculated in the given real part of the optical potential. Doing so, the useful simplifications are usually made. Indeed, in the nucleus-nucleus elastic channel, one has the strong absorption in the inner region $b \le R$, and therefore one needs the correction of the trajectory only at $b \sim R$, where the long-range Coulomb forces are operative. Usually, this is done according to a simple prescription that consists in replacing the impact parameter b by $b_c(b)$, the distance of closest approach of nuclei in the field of the potential $Z_pZ_te^2/r$

$$b \;\rightarrow\; b_c = \bar{a} + \sqrt{\bar{a}^2 + b^2}. \tag{13}$$

Here, $\bar{a} = Z_pZ_te^2/2E_{c.m.}$ is the half-distance of the closest approach of nuclei at $b = 0$.

In Figure 2, one can see from the calculations in [10] that, even at comparatively small charge of the ^{16}O nucleus, the distortion effect manifests itself at energies as high as $E \sim 60$ A/MeV and becomes significant at still lower energies. Thus, the Coulomb distortion of the trajectory shifts the diffraction pattern by the Coulomb deflection angle $\vartheta_c \sim U_B/E$ ($U_B = Z_pZ_te^2/R_C$), thus extending the applicability range of the theory of small-angle scattering within the high-energy approximation.

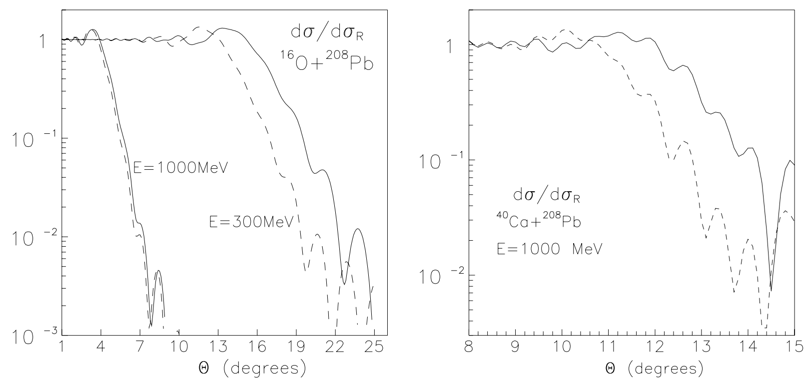

Figure **2.** The influence of the Coulomb trajectory distortion on the elastic differential cross section related to the Rutherford one. Solid and dashed curves are with and without the trajectory shift. Parameters of the Coulomb and symmetrized Woods-Saxon potentials are taken from [10].

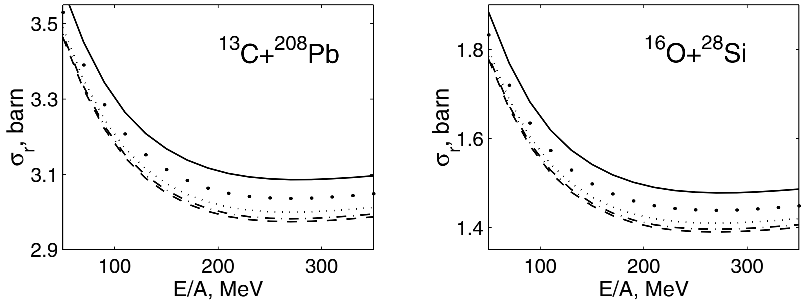

Figure **3.** The in-medium effect on the total reaction cross sections: solid curves – without allowance for medium, boldface dots – $(1/20)\rho_\circ$, dotted curves – $(1/6)\rho_\circ$, dash-dotted – $(1/3)\rho_\circ$, and dashed – at $\rho_\circ$.

When applying the HEA calculations to compare differential cross sections with experimental data one should bear in mind that the ratio $\bar{\alpha}_{NN}$ in the phase (3) is not well known from experimental data, and this involves ambiguities in estimations of the real part of the corresponding amplitude of scattering (1). Otherwise, the NN-total cross section $\bar{\sigma}_{NN}$ is measured in a good accuracy and parametrized as a function of energy, e.g., in [12]. Thus, total reaction nucleus-nucleus cross sections can be calculated in an appropriate way, and below in Section 3, they are performed using the HEA expressions (2) and (3) without reproducing respective optical potentials (4). In detail the respective formulae and methodical analysis of calculations of σ_r are done in [13]. As to methodical results, here we consider only the role of in medium effect on total reaction cross sections accounted for by the factor f_m in the phase (3). This factor depends on ρ and the collision energy, and can be taken in its parametrized form from [14]. The reaction cross sections were calculated in [13] supposing the density ρ not to depend on a distance variable r, i.e. $\rho = \bar{\rho}$.

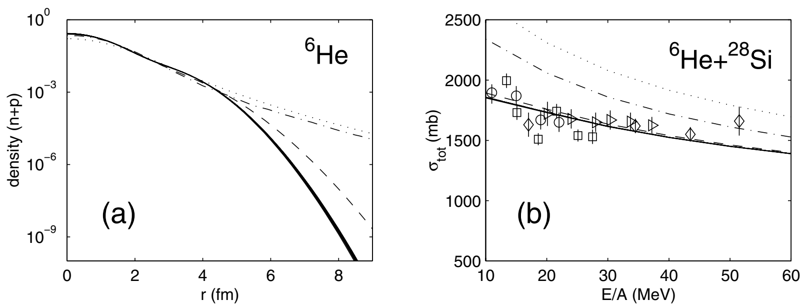

Figure **4.** Matter density distributions for ^{6}He calculated with the COSMA-model (dash-dotted line) and the LSSM-model (dotted line). The M- and T-model densities are given by solid bunch and dashed lines, respectively. b) Total reaction cross-section for ^{6}He+^{28}Si. The curves are as in a).

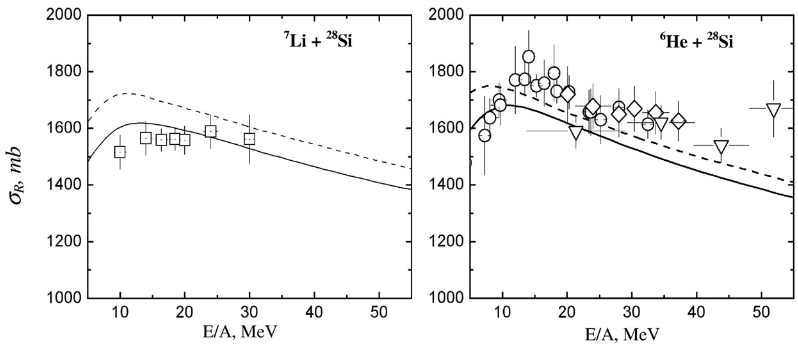

Figure **5.** Total cross sections of reactions of ^{7}Li and ^{6}He with ^{28}Si. Solid curves - the microscopic (DF+H)- model calculations, dashes - the semiphenomenological S-model. Experimental data and calculated curves are from [24].

Figure 3 shows cross sections at different $\bar{\rho} = \rho_p + \rho_t$: $\bar{\rho} = 0$ (solid curves), $\bar{\rho} = (1/20)\rho^\circ$ (boldface dots), $\bar{\rho} = (1/6)\rho^\circ$ (dotted curves), $\bar{\rho} = (1/3)\rho^\circ$ (dash-dotted curves) and $\bar{\rho} = \rho^\circ$ (dashed curves), where $\rho^\circ = \rho_p(0) + \rho_t(0)$. The radii and diffuseness parameters of the pointlike densities in projectile and target nuclei are given in [13]. One can see that the nuclear-medium effect leads to a decrease of 4-7$\%$ in total cross sections, the dependence on the matter density being strongly nonlinear. And it is believed that at lower energies in medium dependence of NN-forces influences more weakly the nuclear total cross sections because the overlapping region of colliding nuclei decreases when the energy decreases.

In Figures 4, 5 we show how one can use calculations of nucleus-nucleus total reaction cross sections for testing density of exotic nuclei when density distributions for the target nuclei are known from other sources. As an example, in Figure 4 are given the results of the calculations [15] of the total reaction cross sections for ^{6}He+^{28}Si at energies $(E/A_p) = 10 \div 40$ MeV using the HEA expressions (2) and (3) with the Coulomb and in-medium corrections included. Comparison with the data from [16, 17] is made. The ^{6}He densities of the COSMA-model [18] (dash-dots)[2], the LSSM-model [20] (dots), the T-model [21] (dashes), and the M-model [22] were applied. The T-model density have the Gaussian asymptotics and its parameters were obtained in [21] by fitting to the data on the total reaction cross section at E(^{6}He)=800 MeV. Otherwise, the COSMA- and LSSM-model densities have extended tails which are related to realistic exponential asymptotics. They result in the enhancement of the corresponding cross-section. The bunch of solid curves corresponds to calculations with a set of parameters of M-model at the rms matter radius of ^{6}He $R_{rms,\,N} = 2.331\,fm$ coincided with the “experimental” rms-radius obtained in [21]. In the other models, the rms-radii are $R_{rms,\,N} = 2.560\,fm$ (COSMA) and $R_{rms,\,N} = 2.956\,fm$ (LSSM). The problem of such a difference

[2] In [15], the applied COSMA-density of ^{6}He is taken with the improved asymptotics from [19] provided by Dr. S. Ershov

between rms radii is discussed in [23] where the coupling of elastic and elastic breakup channels was shown to play an important role in processes with weakly bound nuclei.

In Figure 5, to remove the questions on an applicability of the HEA at energies of tens of MeV/nucleon, calculations are presented for reactions at the same energies but within the DWUCK4 code [5]. Here the microscopic optical potential $U_{opt} = V^{DF} + iW^H$ was calculated in [24] for the reactions ^{7}Li,^{6}He+ ^{28}Si with V^{DF} (7), calculated with the help of the effective Paris NN-potential CDM3Y6, as was explained before, and with the HEA W^H potential (6). For ^{6}He, it was utilized the T-density while for ^{7}Li - the density from [25]. These results from [24] are shown in Figure 5 by solid curves together with the renewed experimental data on reactions ^{7}Li,^{6}He+^{28}Si, obtained in Laboratory of Nuclear Reactions of JINR. The dashed curves are calculations using the semiphenomenological model of Satchler [26] (S-model), where only direct part V^D of the real potential was accounted for together with the phenomenological imaginary part of the potential.

One can conclude that if one applies realistic nuclear densities, then the general features of experimental total reaction cross sections can be explained without introducing free parameters. To explain the data more exactly, one needs to include additional effects on mechanism of nuclear reactions, e.g., the role of nucleon removal processes and of the collective excitation channels.

4 Differential Elastic Cross Sections and Semimicroscopic Optical Potentials

Microscopic optical potentials constructed on the basis of the HEA- and DF-potentials V^H, W^H and V^{DF} in the form of

$$U^H_{opt}(r) \,=\, V^H(r) \,+\, iW^H(r), \tag{14}$$

$$U^F_{opt}(r) = V^{DF}(r) \,+\, iW^H(r) \tag{15}$$

were calculated and applied in [11] and [27] to estimate differential cross sections of elastic scattering of the ^{16}O and ^{17}O heavy ions on various nuclei at energies of about hundred MeV/nucleon and to compare them with existing experimental data [28] and [29], correspondingly. It is emphasized that, from the beginning no free adjustable parameters were introduced. As an example, Figures 6, 7 show such results for the scattering of the ^{16}O nuclei on ^{40}Ca,^{90}Zr at E_{lab}=1503 MeV. Comparison was also made with the phenomenological optical Woods-Saxon potentials $U^P_{opt} = V^P + iW^P$ whose parameters were fitted in [28] with the same experimental data using the code ECIS [6]. Note that our calculations were based on the HEA eqs.(1), (3), (12), (13) both for the microscopic and phenomenological potentials. It is seen that the HEA curves lie rather close to those obtained by numerical solving the wave equation at scattering angles of $\vartheta \simeq 2^\circ - 4^\circ$ – that is, within the applicability range of the HEA method.

If one considers the results of comparison with experimental data in more detail then it can be seen from Figure 7b that the behavior of the imaginary part of W^H (dashed curve) of both the optical potentials (14) and (15) differs markedly from the behavior of the adjusted WS-potential (dotted curve) in the dominant-contribution region at the periphery of interaction. This in turn leads to sizable deviations of behaviors of the corresponding differential cross sections in Figure 7c. The reason of this discrepancy might be due to the nonrealistic slope of the U^H_{opt} potential because of that accounts for only the direct part of nucleus-nucleus interaction. On the other hand, the depths of microscopic potentials are believed to be too large as compared to the usual depths of the fitted phenomenological potentials. Indeed, the simple folding is working well for a comparably weaker densities in the surface region of interaction, while in the inner region the more complicated effects must be taken into consideration. Bearing in mind these circumstances one deems it reasonable to test three possible structures of so-called semimicroscopic optical potentials on the

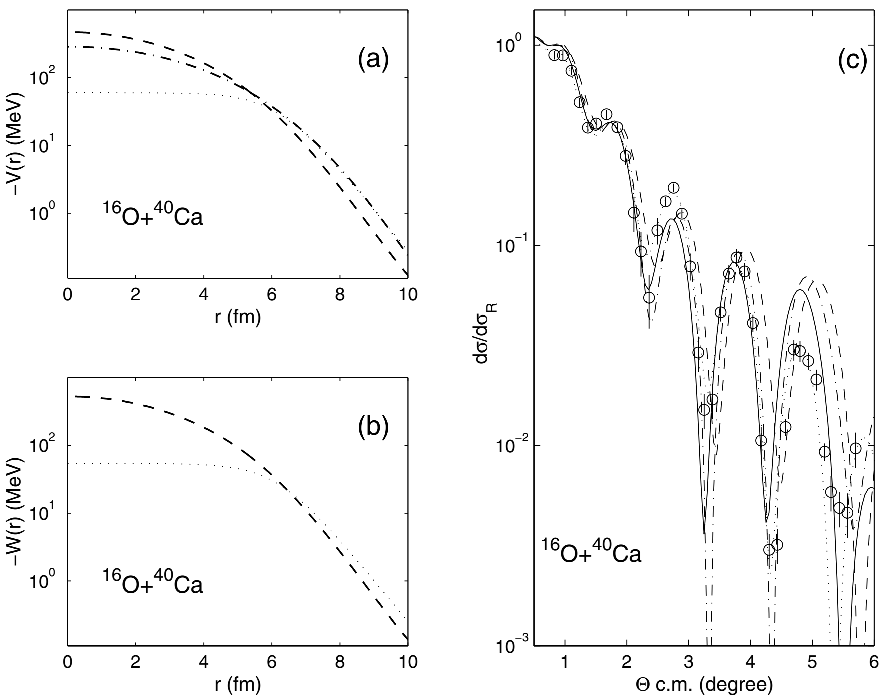

Figure **6.** Optical potentials U^H_{opt} and U^F_{opt} calculated for ^{16}O + ^{40}Ca at $E_{lab}+1503$ MeV: (a) real part of the potential, (b) – the imaginary part, and (c) – the ratio of the calculated cross sections to the Rutherford one. In (a), (b), the dashed curves are for the U^H_{opt}, the dash-dotted curves – for U^F_{opt}, and dotted curves – the Woods-Saxon U^P_{opt} potential. In (c), notations correspond to that given for potentials in (a) and (b), while the circles are experimental data from [28], the solid curve is the HEA calculations for the adjusted U^P_{opt} W-S-potential, and the dotted curve represents the results of the numerical solving of the Schrödinger equation.

basis of microscopic calculations of their individual components, namely,

$$U_{opt}^{A} \;=\; N_r^A\, V^H \;+\; iN_{im}^A\, W^H, \tag{16}$$

$$U_{opt}^{B} \;=\; N_r^B\, V^{DF} \;+\; iN_{im}^B\, W^H, \tag{17}$$

$$U_{opt}^{C} \;=\; N_r^C\, V^{DF} \;+\; iN_{im}^C\, V^{DF}. \tag{18}$$

Thus, each of the potentials involves only two adjustable parameters N_r and N_{im}. As a matter of fact, their variation leads to a change in the strength of each of the two components and to their shift towards the center or away from it.

In [11] and [27], differential cross sections of ^{16,17}O on various target nuclei were calculated by using these semimicroscopic potentials, and the coefficients N_r and N_{im} were determined from a comparison with the experimental data [28], [29]. Figure 8 exhibits the respective results only for scattering of ^{17}O when using the potential $U_{opt}^{C} = N_r^C\, V^{DF} + iN_{im}^C\, V^{DF}$ with the coefficients N_r and N_{im} proved to be, respectively, 0.6 and 0.6 for ^{60}Ni; 0.6 and 0.5 for ^{90}Zr; 0.5 and 0.5 for ^{120}Sn; 0.5 and 0.8 for ^{208}Pb. The agreements with experimental data appear to be reasonably good if one considers that calculations were made in the framework of HEA, with the result that, at angles beyond its applicability range, there are moderate discrepancies with experimental data.

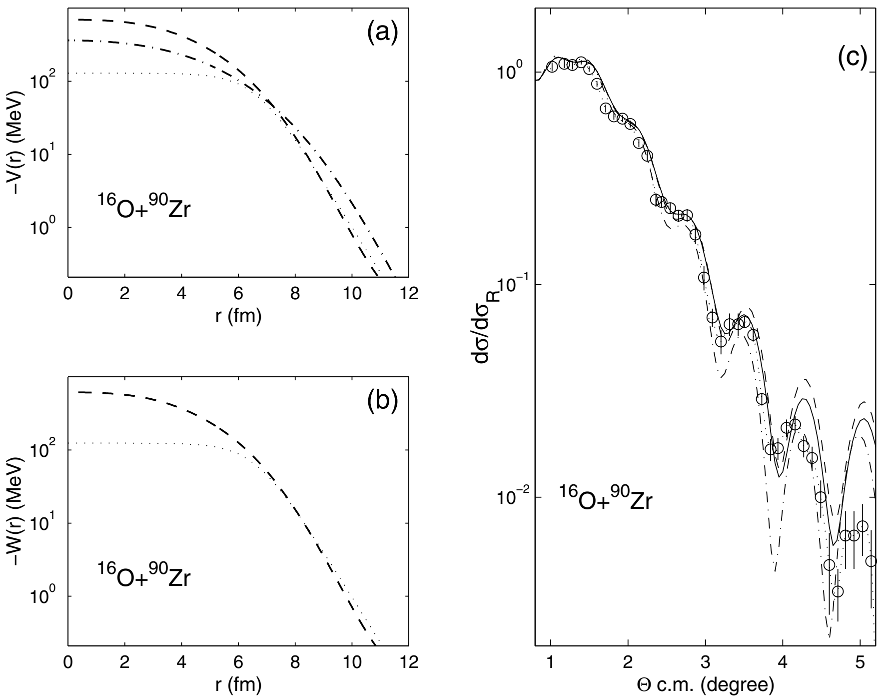

Figure **7.** The same as in Figure 6, but for ^{16}O+^{90}Zr.

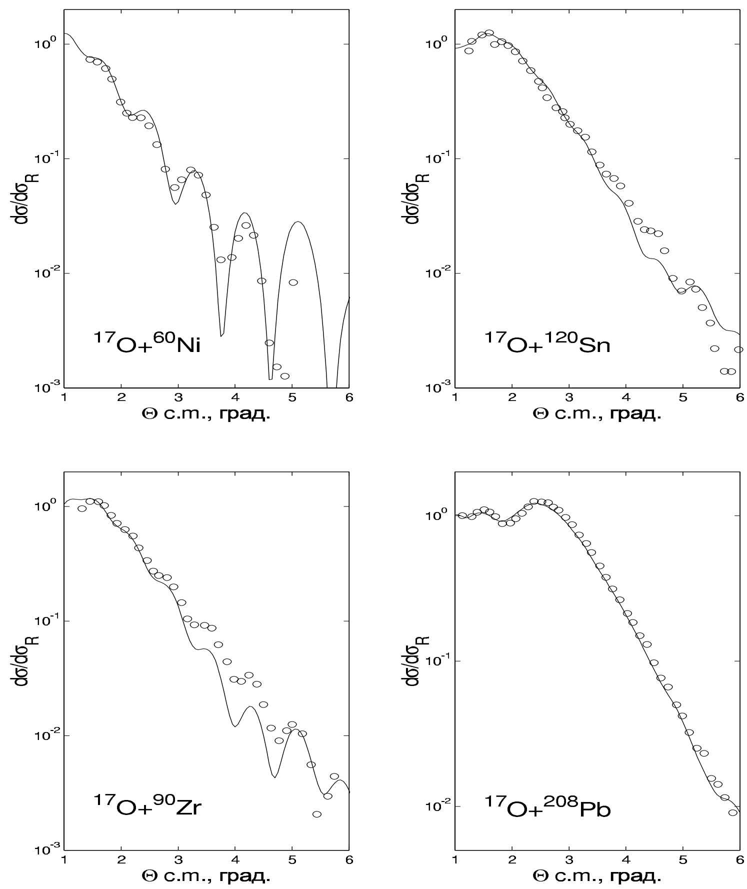

Figure **8.** Ratio of the differential cross sections for elastic scattering of ^{17}O on various target-nuclei to the Rutherford one according to calculations with semimicroscopic optical potentials (see the text) at $F_{lab} = 1435$ MeV along with experimental data from [29].

5 Summary

The microscopic approaches to construct optical potentials are most useful because they are based on known amplitudes and cross sections of nucleon-nucleon scattering and on density distributions of colliding nuclei. In this way, in principle, one can establish the dependence of nuclear cross sections on the energy and on the kind of interacting nuclei. The theory makes it possible to see basic features of mechanism of nucleus-nucleus scattering, in particular, the leading role of the nuclear periphery, the need for taking into account distortion of the trajectory, and the requirement of introducing the in medium dependence of effective NN-forces taking part in calculating nucleus-nucleus potentials. One can derive the HEA microscopic optical potential which is perfectly analogous to that of the HEA microscopic diffraction theory, but the HEA-potential itself can be also tested at lower energy when one uses numerical codes of solving the Schrödinger equation to study scattering processes. At present one can construct semimicroscopic optical potentials whose asymptotic coincides with that of microscopic potentials and which introduce only few (say, two) free parameters,in particular, the absolute values of their real and imaginary parts adjusted in a comparison with experimental data. The construction of such nucleus-nucleus potentials removes the known problem of ambiguity of parameters of phenomenological potentials. Besides, the developed theory of scattering of nuclei allows one to study the exotic nuclei, because the microscopic potentials depend on the shape of their densities and thus it can be tested by involving different models under consideration.

References

1. R. J. Glauber, *Lectures on Theoretical Physics* (Interscience, New York, 1959) p.315.
2. A. G. Sitenko, *Ukr. Fiz. Zhurnal* **4**, 152 (1959).
3. W. Czyz and L. S. Maximon, *Ann. Phys.* **52**, 59 (1969).
4. J. Formanek, *Nucl. Phys. B* **12**, 441 (1969).
5. P. D. Kunz and E. Rost, *Computational Nuclear Physics* Vol.2, Eds: K. Langanke et al. (Springer Verlag, 1993) p.88.
6. J. Raynal *Phys. Rev. C* **23**, 2571 (1981); *see also* J. Raynal, *Computing as a Language of Prysics* (IAEA, Vienna, 1972) p.75.
7. V. K. Lukyanov, *Phys. At. Nucl.* **69**, 1033 (2006).
8. D. T. Khoa and G. R. Satchler, *Nucl. Phys. A* **668**, 3 (2000).
9. M. Avrigeanu, G. S. Anagnostatos, A. N. Antonov, and J. Giapitzakis, *Phys. Rev. C* **62**, 017001 (2000); M. Avrigeanu, G. S. Anagnastatos, A. N. Antonov, and V. Avrigeanu, *Int. J. Mod. Phys. E* **11**, no.3, 249 (2002).
10. V. K. Lukyanov and E. V. Zemlyanaya, *Int. J. Mod. Phys. E* **10**, 169 (2001).
11. V. K. Lukyanov, E. V. Zemlyanaya, and K. V. Lukyanov, *Phys. At. Nucl.* **69**, 240 (2006).
12. S. Charagi and G. Gupta, *Phys. Rev. C* **41**, 1610 (1990).
13. V. K. Lukyanov, E. V. Zemlyanaya, and B. Słowiński, *Phys. At. Nucl.* **67**, 1282 (2004).
14. Cai Xiangzhou *et al*., *Phys. Rev. C* **58**, 572 (1998).
15. V. K. Lukyanov *et al*., *Int. J. Mod. Phys. E* **13**, 573 (2004).
16. R. E. Warner *et al*., *Phys. Rev. C* **52**, R1166 (1995).
17. I. V. Kuznetsov *et al*., *Yad. Fiz.* **65**, 1609 (2002).
18. M. V. Zhukov *et al*., *Phys. Rep.* **231**, 151 (1993).
19. S. N. Ershov *et al*., *Phys. Rev. C* **56**, 1483 (1997).
20. S. Karataglidis *et al*., Phys. Rev. C **61**, 024319 (2000).
21. I. Tanihata *et al*., *Phys. Lett. B* **289**, 261 (1992).
22. S. E. Massen and Ch. C. Moustakidis, *Phys. Rev. C* **60**, 0240005 (2000); Ch. C. Moustakidis and S. E. Massen, *Phys. Rev. C* **64**, 014314 (2000).
23. J. S. Al-Khalili, J. A. Tostevin, and I. J. Thompson, *Phys. Rev. C* **54**, 1843 (1996).
24. Yu. G. Sobolev *et al*., *Izv. Akad. Nauk, Ser. Fiz.* **69**, no.11, 1603 (2005).
25. M. El-Azab Farid and M. A. Hassanain, *Nucl. Phys. A* **678**, 39 (2000).
26. R. J. Satchler, *Nucl. Phys. A* **579**, 241 (1988).
27. E. V. Zemlyanaya *et al*., *Izv. Akad. Nauk, Ser. Fiz.* **69**, no.11, 1651 (2005); `nucl-th/0412026`.
28. P. Roussel-Chomaz *et al*., *Nucl. Phys. A* **477**, 345 (1988).
29. R. Liguori Neto *et al*., *Nucl. Phys. A* **560**, 733 (1993).